



CHALMERS
UNIVERSITY OF TECHNOLOGY

Modeling Sulfite Oxidation Reactions in Co-Absorption of Nitrogen Oxides and Sulfur Oxides

Downloaded from: <https://research.chalmers.se>, 2026-03-17 05:35 UTC

Citation for the original published paper (version of record):

Aprilia, R., Johansson, J., Normann, F. (2025). Modeling Sulfite Oxidation Reactions in Co-Absorption of Nitrogen Oxides and Sulfur Oxides. *Industrial & Engineering Chemistry Research*, 64(51): 24516-24527. <http://dx.doi.org/10.1021/acs.iecr.5c03944>

N.B. When citing this work, cite the original published paper.

Modeling Sulfite Oxidation Reactions in Co-Absorption of Nitrogen Oxides and Sulfur Oxides

Rosa C. Aprilia,* Jakob Johansson, and Fredrik Normann



Cite This: *Ind. Eng. Chem. Res.* 2025, 64, 24516–24527



Read Online

ACCESS |



Metrics & More

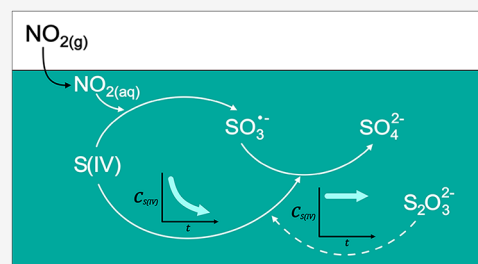


Article Recommendations



Supporting Information

ABSTRACT: Novel mechanisms for sulfite oxidation in a system with nitrogen dioxide ($\text{NO}_{2(\text{g})}$) and thiosulfate are proposed. The oxidation reaction is of particular interest as it drives the depletion of sulfite, which leads to economic challenges in a system designed for the coremoval of nitrogen oxides (NO_x) and sulfur oxides (SO_x). New reaction sets that capture sulfite radical chain oxidation by NO_2 are formulated by integrating previously reported mechanisms and experimental observations. Two new mechanisms are presented with regard to sulfite oxidation by NO_2 . The sulfur radical reaction set describes the sequence of radicals that result in the rapid consumption of sulfite. This mechanism is simplified into a single global reaction, to allow integration into the process modeling software. For the system involving thiosulfate, two reaction sets are proposed, where the presence of polythionate intermediates is evaluated. Kinetic expressions are estimated by fitting the calculated and measured sulfite concentrations, where an error in the range of 1.07–2.41 mol/m³ is achieved. The sensitivity analysis indicates that NO_2 absorption predictions are strongly affected by mass transfer parameters, whereas their impact on the liquid-phase is of low significance.



1. INTRODUCTION

This paper is concerned with the aqueous oxidation of S(IV) ions (SO_3^{2-} and HSO_3^-) in the presence of gaseous nitrogen oxides (NO_x) and supporting chemicals (thiosulfate) for radical scavenging. Previous work has shown that the rate of oxidation of S(IV) ions increases dramatically in the presence of NO_x .^{1–4} However, reaction mechanisms that describe the chemistry of this phenomenon are lacking,^{2,3} which pose a challenge in the development of a coremoval system for NO_x and SO_x , a process where S(IV) oxidation largely governs performance. In optimizing the absorption-based technology, which offers comparable absorption level to the current best available technology for both pollutants,¹ understanding the oxidation rate of S(IV) ions is key to gain process control and achieve an economically viable process.^{5,6}

The oxidation reactions of S(IV) species have been studied extensively, mainly due to past concerns regarding SO_2 emissions and the impacts on atmospheric chemistry that they entail.^{3,7} These species also play a pivotal role in flue gas desulfurization (FGD), where S(IV) ions are formed as intermediates during the absorption of SO_2 from exhaust gases. S(IV) ions initially appear in the system as products of SO_2 dissolution in water. In the aqueous phase, the sulfur species converts $\text{NO}_{2(\text{aq})}$ into nitrous ions (NO_2^-), while simultaneously being oxidized into sulfate (SO_4^{2-}). This interaction significantly enhances NO_2 absorption, with a 200% increase observed when using a 1 mM sulfite solution compared to pure water.⁶ Modeling work carried out by Johansson et al.⁸ has highlighted the dependency of the absorption rate on the molar ratio of S(IV) to $\text{NO}_{2(\text{g})}$. As a

higher S(IV) concentration is associated with a higher level of NO_2 removal, the use of sulfite salts (Na_2SO_3) as additives has been studied, revealing a significant improvement in efficiency.⁹ However, maintaining the absorption level has been identified as a major challenge for the process, as the rapid depletion of sulfite potentially leads to a high operational cost. Therefore, understanding the mechanism involving S(IV) ions is a crucial step in designing a cost-effective process.

The interaction between nitrogen and sulfur species in a liquid phase has attracted much attention due to its poorly understood mechanism. In the absence of NO_2 in the gas phase, the mechanism of sulfite oxidation by oxygen alone is a subject of debate. This is due to the sensitivity of the reaction to impurities, which can either catalyze or inhibit the reaction.^{10–12} The presence of nitrogen in the system further complicates the S(IV) ion oxidation process, as the number of possible reactions increases significantly.^{13–15} Takeuchi et al.¹ investigated the effect of oxygen on the rate of NO_2 absorption with an aqueous solution of sodium sulfite. Oxygen was included in the system by diluting NO_2 in air, which increased the sulfite depletion rate and gave a 40% lower NO_2 absorption rate compared to when NO_2 was diluted in nitrogen. The

Received: September 19, 2025

Revised: December 1, 2025

Accepted: December 3, 2025

Published: December 12, 2025



kinetics of the reaction between oxygen and sulfite cannot explain the significant decrease in NO_2 absorption rate, since studies have reported a low rate constant.^{16,17} It has been suggested that a reaction mechanism that involves radical chains of sulfite is a reasonable explanation for this phenomenon. Johansson et al.⁴ have demonstrated a significant increase in the S(IV) oxidation rate in the presence of $\text{NO}_{2(g)}$. Littlejohn et al.² and Clifton et al.^{2,3} have investigated the behavior of the system under a range of conditions and proposed different mechanisms for the reaction to proceed, although the radical chain reaction and its kinetics remain poorly understood.

In FGD processes, sulfite oxidation facilitates gypsum saturation, which leads to scaling and reduced process performance.¹⁸ This issue has been addressed by adding radical-scavenging species, such as thiosulfate salts ($\text{Na}_2\text{S}_2\text{O}_3$). The effects of thiosulfate addition in a system with S(IV) ions and gaseous NO_2 have been demonstrated in a study by Johansson et al.,⁴ whereby in the presence of thiosulfate, the rate of S(IV) consumption decreased by a factor of 12. Since NO_2 absorption is primarily governed by the concentration of S(IV) ions, the radical-scavenging additive also positively affects the absorption level, such that absorption was maintained at 70% after 2.5 h of operation. These results suggest a substantial improvement, in contrast to the results obtained in an experiment without thiosulfate, in which only 15% of the NO_2 absorption remained at the end of the run. Compared to the desulfurization process, in which thiosulfate makeup is a constant requirement, thiosulfate has been shown to be more stable in the NO_x and SO_x absorption system due to the less-acidic environment.¹⁸ In the experiment with only thiosulfate and oxygen, no clear signs of oxidation were observed, while only a low level of thiosulfate consumption was observed in the presence of $\text{NO}_{2(g)}$ and S(IV) ions.⁴ Given its significant role, understanding the thiosulfate radical-scavenging mechanism is highly relevant to the design of the coabsorption system.

To design an economically feasible process, it is necessary to understand the chemistry of the interaction between nitrogen and sulfur, in order to optimize the consumption of chemicals and reduce the process cost. Understanding the reaction would also allow adaptation to a wide range of processes with different working conditions. This work suggests new reaction mechanism to address the role of radical species on the oxidation of S(IV) ions. The obtained kinetics for the new mechanism, along with reported values in the literature,¹⁹ are applied to a reactor model that emulates the experimental investigation of S(IV) oxidation in the presence of $\text{NO}_{2(g)}$ carried out by Johansson et al.,⁴ with the aim of providing deeper insights into the system's behavior. The reaction mechanism is described in Section 2, where recent findings relevant to the system's chemistry are summarized. Section 3 discusses the approach of the present study, describing the reactor configurations and mass transfer models in the simulation, which have significant roles on the resulting concentration profile. Finally, the results are presented in Section 4, where the key challenges to understanding the reaction will be identified and suggestions for future applications will be made.

2. CHEMISTRY

This work focuses on the oxidation of S(IV) ions in the presence of oxygen and $\text{NO}_{2(g)}$, as well as the radical

scavenging reaction involving thiosulfate. The overall reaction mechanism is illustrated in Figure 1.

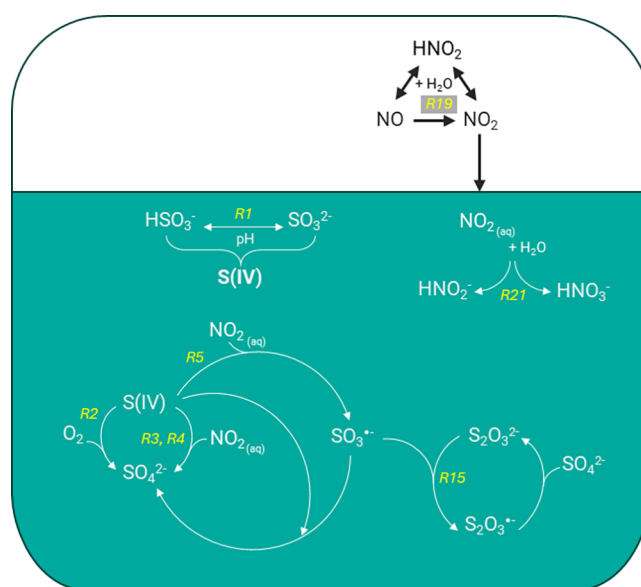


Figure 1. Overall reaction mechanism of S(IV) oxidation in the presence of $\text{NO}_{2(g)}$. Reaction labels are denoted in yellow.

In the aqueous phase, HSO_3^- is in equilibrium with SO_3^{2-} based on the instantaneous Reaction R1²⁰



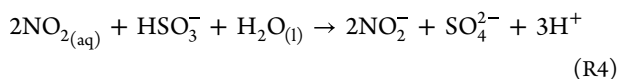
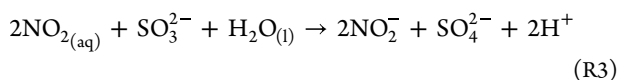
Thus, the distribution of S(IV) species is pH-determined, with HSO_3^- being the dominant species up to pH 6, while a further increase in pH causes an increase in the concentration of SO_3^{2-} ions. In the presence of oxygen, SO_3^{2-} is oxidized to SO_4^{2-} according to R2²¹



While the oxidation of SO_3^{2-} by oxygen has been widely studied, consensus is lacking. Sivaji et al.¹⁰ have argued that the rate of reaction depends on the type of equipment, the pH of the solution, and the concentrations of O_2 and sulfite, along with the purity of sulfite. The effects of impurities were further explored by Linek and Mayrhoferová,¹¹ who found that the rate was lower when a solution of commercial Na_2SO_3 was used instead of absorbing gaseous SO_2 into agitated NaOH, and this was attributed to higher levels of inhibitory impurities in the commercial Na_2SO_3 .

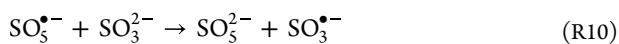
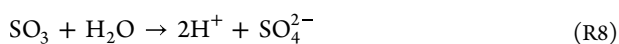
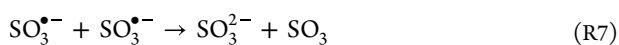
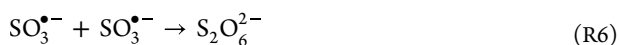
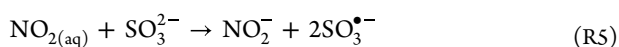
There is general agreement among research groups regarding the influences of S(IV) concentration and pH, with the values for both parameters being shown to be proportional to the rate of reaction. However, there is a lack of consistency regarding the effect of the oxygen concentration, reported variously as zero-order for oxygen, half-order with respect to the initial oxygen concentration, or half-order with varying oxygen concentration. The sensitivity of the reaction has been described in a review by Linek et al.,²² with a broad spectrum of rate constants and orders of concentration being noted in publications describing various experimental setups and reaction conditions. Despite the wide discrepancies in the reported kinetics, the reaction is widely regarded as pseudo-first order with respect to sulfite,^{20,21,23–25} as summarized by Beilke et al.²⁰

The interactions between S(IV) ions and NO_{2(aq)} are important, as NO₂ absorption is shown to be dependent upon the S(IV) concentration.^{8,26} For this system, Clifton et al.³ have suggested the overall Reactions R3 and R4 for the interactions between NO_{2(aq)} and S(IV)



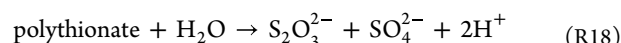
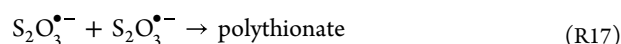
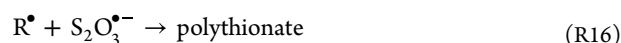
Reactions R3 and R4 have been reported to be dependent upon gaseous NO₂ concentrations in the range of 0.3–50 ppm, proving that R3 and R4 are in a kinetically controlled regime. A recent study performed by Sapkota et al.¹⁴ confirmed this finding in an investigation using the NO_{2(g)} concentration range of 2–10 ppm. Littlejohn et al.² investigated a range of pH as well as the NO₂, S(IV), and oxygen concentrations, using Raman spectroscopy to determine the product concentrations throughout the experiment. The results suggest that in the higher range of NO₂ concentration, i.e., 1000–5000 ppm, the oxidation rate is limited by the transfer of oxygen into the solution. As research studies using the intermediate and higher ranges of NO₂ concentrations are lacking, the question remains as to the role of mass transfer for NO₂ concentrations higher than 50 ppm. As with the oxidation of S(IV) by oxygen, there is good agreement on the influences of S(IV) concentration and pH level on the rate of reaction. It has been reported that the rate of reaction increases with increasing concentration of S(IV) and increasing pH level.^{2,3,6}

It has been shown that the rate of S(IV) depletion in a system with NO_{2(g)} occurs more rapidly than the concurrent absorption of NO₂.^{14,27} The oxidation rate is also significantly faster than the sole oxidation of S(IV) by oxygen (R2),²⁷ and it is also faster than the proposed rates for R3 and R4. In experiments, Littlejohn et al.² have observed that for every mole of NO₂ absorbed, at least 4 mol of sulfite are consumed in the presence of oxygen. Johansson et al.⁴ have reported a more-significant increase in the S(IV) oxidation rate, in which the molar ratio of oxidized S(IV) to absorbed NO₂ is >30. These results suggest that NO₂ initiates a radical chain reaction, which explains the high-level consumption of S(IV) species. Littlejohn et al.² have proposed the following radical chain reaction mechanism



R5–R8 are suggested to represent the reaction mechanism in the absence of O₂, as more S₂O₆²⁻ is found in the product. As O₂ is added to the system, the proportion of SO₄²⁻ increases and the complete mechanism (R5–R14) operates.

An oxidation inhibitor, namely thiosulfate S₂O₃²⁻, is then considered as an additive for the system. In the FGD process, S₂O₃²⁻ is known to act as an effective radical scavenger. Laboratory-scale²⁸ and pilot-scale^{18,29} studies of thiosulfate in the FGD process have revealed lower rates of sulfite oxidation and sulfate production, which reduce the level of scaling on the scrubber. Mo et al.²⁸ have proposed the following mechanism for thiosulfate inhibition



Reactions R15 and R16 will scavenge the radical species, breaking the radical chain reaction that starts with R5. Thereafter, R17 occurs, which significantly reduces sulfite consumption.

In the context of NO₂ absorption, Sapkota et al.¹⁴ have investigated the effect of thiosulfate on the sulfite oxidation rate at low NO_{2(g)} concentrations in the range of 2–10 ppm. For 40 mM sulfite, the addition of 25 or 100 mM thiosulfate reduced the oxidation rate by 1 order of magnitude, without any significant effect from the increased thiosulfate concentration. Johansson et al.⁴ performed an online monitoring experiment to investigate the transient profiles of different reactions, involving 40 mM of S(IV), 40 mM of thiosulfate, and 100 ppm of NO₂ with interchanging species in the system. When the rates of reaction of S(IV) oxidation by O₂ with and without thiosulfate were compared it was clear that thiosulfate inhibited the oxidation reaction, as the S(IV) concentration remained stable and no formation of sulfate was observed.

The rate of S(IV) oxidation by NO₂ is also reduced when thiosulfate is present in the system. In the absence of S(IV), a solution with only thiosulfate results initially in 60% NO₂ absorption, followed by a gradual decrease to 40% at the end of the experiment. The study of Schmid et al.⁶ supports this finding by comparing the rates of NO₂ absorption in water to different concentrations of thiosulfate, with a slight increase in NO₂ absorption observed when thiosulfate is added. In this investigation, 50 ppm of NO₂ was absorbed to 2, 5, and 10 mM of sulfite, within a range of 1–100 mM of thiosulfate. The study shows that adding more than 2 mM thiosulfate results in a minor reduction of the sulfite oxidation reaction. The addition of thiosulfate brings the reaction rate to a level similar to those observed when varying the sulfite concentration.

3. METHOD

This work proposes a reduced reaction mechanism to describe S(IV) ion oxidation in a system that contains O₂, NO₂ and thiosulfate, to complement the reduced mechanism for nitrogen and sulfur reported by Ajdari et al.¹⁹ The proposed mechanisms are implemented in a reactor model, where the rate constants are fitted to the experimental data from Johansson et al.⁴ The experimental work is briefly described

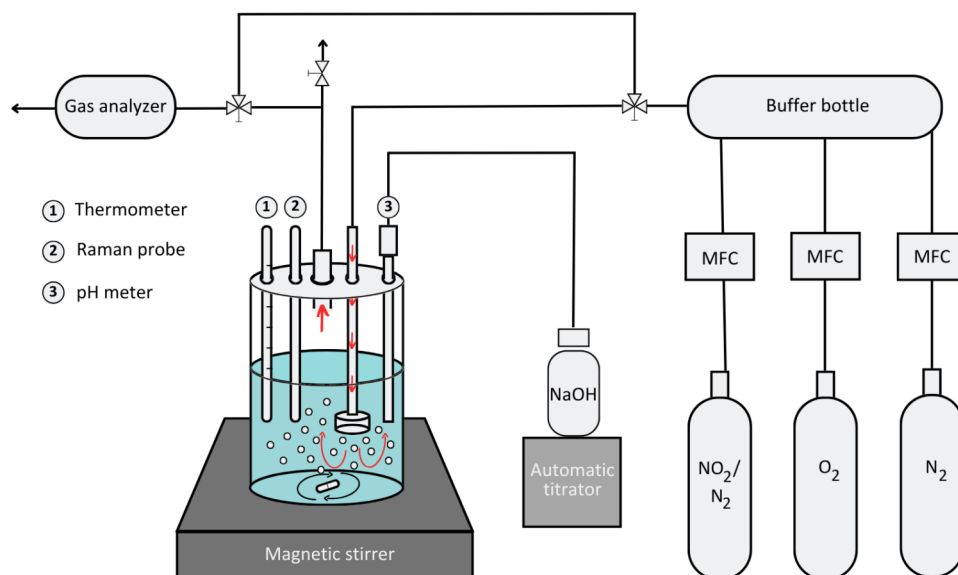


Figure 2. Illustration of the experimental setup described by Johansson et al.⁴ MFC, Mass flow controller.

Table 1. Experimental Matrix Used in the Work of Johansson et al.^{a4}

investigation	liquid concentration (mol/m ³)						gas concentration	
	SO ₃ ²⁻	HSO ₃ ⁻	HSO ₄ ²⁻	S ₂ O ₃ ²⁻	NO ₂ ⁻	CO ₃ ²⁻	NO ₂ (ppm)	O ₂ (%)
0 ^b	-	-	-	-	-	-	95	3
1	20	20	-	-	-	-	-	3
4	20	20	-	-	-	-	95	3
6	20	20	-	40	-	-	95	3

^aThe numbering is retained from the original work, although not all investigations are used in the present work. ^bUnpublished results, data used for mass transfer parameter fitting.

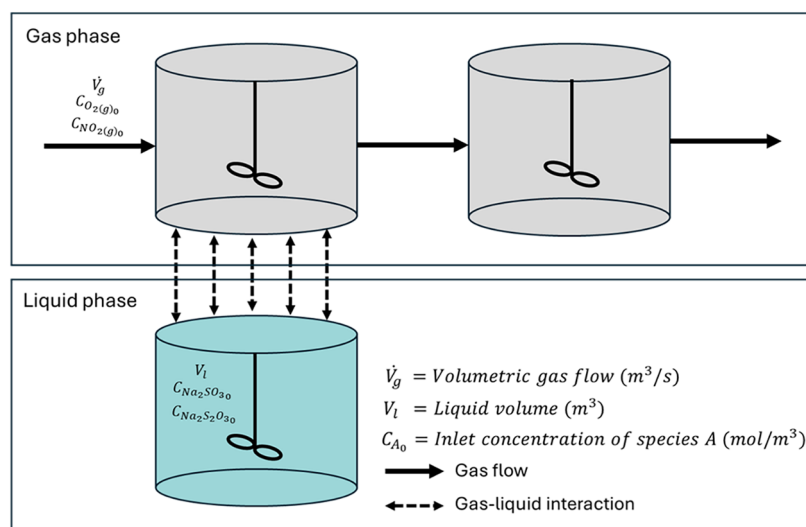


Figure 3. Schematic of the reactor model. Gas flow denoted by solid arrow. Gas–liquid interaction denoted by dashed arrow.

in Subsection Experimental, followed by a description of the model in Subsection Model Description. Finally, the proposed reaction pathways and their kinetic parameter approximation are discussed in Subsection Proposed Mechanism.

3.1. Experimental Section. The experimental work of Johansson et al.⁴ investigated the influence of NO₂ and thiosulfate on the S(IV) oxidation reaction. A notable improvement made in this study is the online measurement of concentrations using Raman spectroscopy. This method

allows continuous monitoring of the liquid concentrations in the setup, providing new insights into the behavior of the complex system of nitrogen and sulfur.

The experimental setup is illustrated in Figure 2. The gases were premixed from 1% NO₂ in N₂, N₂ and O₂ before flowing into an Erlenmeyer bottle that contained prepared batch solutions of S(IV) salts and/or thiosulfate. The pH electrode was connected to a titrator (905 Titrando; Metrohm), which was programmed to maintain a pH level of 7 by adding 0.1 M

Table 2. Kinetic Expressions Used in the Model, as Proposed by Ajdari et al.¹⁹

	reaction	kinetic expression (mol/m ³ /s)
Liquid-Phase Reaction		
R1	$\text{HSO}_3^- \leftrightarrow \text{H}^+ + \text{SO}_3^{2-}$	$r_1 = k_{\text{ins}} \left(C_{\text{HSO}_3^-} - \frac{C_{\text{H}^+} C_{\text{SO}_3^{2-}}}{K_{\text{eq},2}} \right)$
R2	$2\text{SO}_3^{2-} + \text{O}_{2(\text{aq})} \rightarrow 2\text{SO}_4^{2-}$	$r_{2,298} = 1.2 \times 10^{-4} C_{\text{H}^+}^{-0.16} C_{\text{SO}_3^{2-}}$
R3	$2\text{NO}_{2(\text{aq})} + \text{SO}_3^{2-} + \text{H}_2\text{O}_{(\text{l})} \rightarrow 2\text{NO}_2^- + \text{SO}_4^{2-} + 2\text{H}^+$	$r_3 + r_4 = k_{\text{pH}} C_{\text{NO}_2} (C_{\text{SO}_3^{2-}} + C_{\text{HSO}_3^-})$
R4	$2\text{NO}_{2(\text{aq})} + \text{HSO}_3^- + \text{H}_2\text{O}_{(\text{l})} \rightarrow 2\text{NO}_2^- + \text{SO}_4^{2-} + 3\text{H}^+$	
R19	$\text{SO}_{2(\text{aq})} + \text{H}_2\text{O}_{(\text{l})} \leftrightarrow \text{H}^+ + \text{HSO}_3^-$ (R19)	$r_{19} = k_{\text{ins}} \left(C_{\text{SO}_2} - \frac{C_{\text{H}^+} C_{\text{HSO}_3^-}}{K_{\text{eq},1}} \right)$
R20	$2\text{NO}_{2(\text{aq})} + \text{H}_2\text{O}_{(\text{l})} \rightarrow \text{HNO}_{2(\text{aq})} + \text{HNO}_{3(\text{aq})}$ (R20)	$r_{20,298} = 1 \times 10^5 C_{\text{NO}_2}^2$
R21	$2\text{HNO}_{2(\text{aq})} \leftrightarrow \text{NO}_2 + \text{NO} + \text{H}_2\text{O}$ (R21)	$r_{21,298} = 13.4 C_{\text{HNO}_{2(\text{aq})}}^2 - 1.6 \times 10^8 C_{\text{NO}_{2(\text{aq})}} C_{\text{NO}_{(\text{aq})}}$
R22	$\text{HNO}_{2(\text{aq})} \leftrightarrow \text{H}^+ + \text{NO}_2^-$ (R22)	$r_{22} = k_{\text{ins}} \left(C_{\text{HNO}_2} - \frac{C_{\text{H}^+} C_{\text{NO}_2^-}}{K_{\text{eq},6}} \right)$
R23	$\text{HNO}_{3(\text{aq})} \leftrightarrow \text{H}^+ + \text{NO}_3^-$ (R23)	$r_{23} = k_{\text{ins}} \left(C_{\text{HNO}_3} - \frac{C_{\text{H}^+} C_{\text{NO}_3^-}}{K_{\text{eq},7}} \right)$
Gas-Phase Reaction		
R24	$2\text{HNO}_{2(\text{g})} \leftrightarrow \text{NO}_{2(\text{g})} + \text{NO}_{(\text{g})} + \text{H}_2\text{O}_{(\text{g})}$ (R24)	$r_{24} = k_{\text{acid}} \left(C_{\text{NO}} C_{\text{NO}_2} C_{\text{H}_2\text{O}} - \frac{C_{\text{HNO}_2}^2}{K_{\text{eq},8}} \right)$

of NaOH. The Testo 350 gas analyzer from Nordtec, which employs electrochemical sensors based on selective potentiometry, was used to determine the SO₂, O₂, NO, and NO₂ concentrations. The NO₂ absorption level was determined by calculating the difference between the measured outlet concentration and the quantity injected.

The experiments relevant to the present work are summarized in Table 1. The experimental matrix was designed to evaluate the system's behavior following the introduction of new species. In Investigation 0, NO₂ dissolution into water was observed, no sulfur species is present in the system. Investigation 1 was designed to establish the rate of S(IV) oxidation by oxygen, i.e., without the presence of NO_{2(g)}. NO_{2(g)} was introduced in Investigation 4 and thiosulfate was introduced in Investigation 6.

3.2. Model Description. The setup of the reactor model follows the work of Normann et al.³⁰ The gas flow is modeled as two continuous stirred tank reactors (CSTR), and the liquid solution is represented as a batch reactor, as illustrated in Figure 3. The first CSTR is coupled to the batch liquid reactor, in order to simulate the gas–liquid interaction. The outlet concentration of the gaseous phase then further reacts in the second CSTR to capture the gas-phase reaction occurring in the headspace above the liquid.

The gas concentration in the gas–liquid CSTR is defined as

$$\frac{dC_A}{dt} = \frac{1}{V_g} (V_g C_{A0} - V_g C_A) + \sum v_{A,j} r_j + J_A \quad (1)$$

where C_{A0} is the inlet concentration, v_{A,j} is the stoichiometric coefficient of species A in reaction j, r_j is the rate of reaction j in (mol/m³)/s, and V_g corresponds to the volume of gas bubbles inside the liquid described as

$$V_g = \left(\frac{V_1}{1 - \epsilon} \right) \epsilon \quad (2)$$

J_A is the molar flux of species A in mol/m³-gas/s defined as

$$J_A = a \left(\frac{1}{k_{gA}} + \frac{1}{k_{lA}} \right) (C_A^* - C_A) \quad (3)$$

where a is the interfacial area, C_A^{*} is the concentration of species A in equilibrium with its partial pressure at bulk gas (P_A), k_{gA} is the gaseous-phase mass transfer coefficient, and k_{lA} is the liquid-phase mass transfer coefficient.

The mass transfer is defined with a two-film model, in which Henry's law constant is used to determine the concentration of species A in the liquid-phase. A bubble diameter of 5 mm is assumed, so k_{lA} is determined with the correlation described by Kawase and Moo-Young³¹ for a bubble diameter (d_b) greater than 2.5 mm

$$k_{lA} = 0.42 D_{AB}^{1/2} \left(\frac{\rho_1^{1/2} g}{\mu_1^{1/2}} \right)^{1/3} \quad (4)$$

k_{gA} is estimated with the correlation of Cho and Wakao³² for a 3 porous tube sparger

$$k_{gA} = 2.6 \cdot 10^3 D_{AB}^{0.5} v_{SG}^{0.76} \quad (5)$$

Given that NO₂ mass transfer is accompanied by reactions, the Hatta number is used to assess the kinetic regime for reactions involving NO_{2(aq)}. The Hatta number is determined by the following expression for a second-order reaction

$$\text{Ha} = \frac{(D_{Al} k_A C_{Bb})^{0.5}}{k_{Al}} \quad (6)$$

An overall enhancement factor is then calculated based on the correlation of Versteeg et al.³³ for reactions occurring in the liquid film ($Ha > 3$), in which the individual enhancement factor for reaction j (E_j) is defined as

$$E_j = 1 + \frac{D_{Bl}C_{Bb}}{bD_{Al}C_{Ai}} \quad (7)$$

The single-phase CSTR is described by a modified form of eq 1, omitting the mass transfer term (J_A) and replacing the bubble volume (V_g) with the headspace volume (V_{dr}). In the batch reactor, the liquid-phase concentration is described as follows:

$$\frac{dC_A}{dt} = \sum v_{A,j}r_j + J_A\varepsilon \quad (8)$$

where ε is the gas holdup determined with the correlation from Akita and Yoshida.⁹

The mechanism reported by Ajdari et al.^{15,19} for pH 5 was used as the reference mechanism in the model. The reactions and their kinetic expression are summarized in Table 2, and the relevant constants are summarized in Table 3.

Table 3. Key Constants Used in the Model

Coefficient (m ³ , mole, K)
$k_{acid} = 1.4473 \times 10^{-11}$
$k_{ins} = 10^6$
$k_{pH} = 2 \times 10^3$
Gas phase equilibrium constant (m ³ , mole)
$K_{eq,g} = 1.825 \times 10^{-15} e^{4723/T}$
Liquid phase equilibrium constant @298 K (m ³ , mole)
$K_{eq,1} = 14.49$
$K_{eq,2} = 7.0835 \times 10^{-5}$
$K_{eq,6} = 0.51$
$K_{eq,7} = 1.54 \times 10^4$
Henry's law constants (mol/liter/bar)
$H_{NO_2} = 1.21 \times 10^{-4}$
$H_{O_2} = 1.3 \times 10^{-5}$
$H_{HNO_2} = 0.5042$
$H_{HNO_3} = 2.13 \times 10^3$
$H_{H_2SO_4} = 0.01$

3.3. Proposed Mechanism. Table 4 summarizes the reaction sets proposed to describe liquid-phase oxidation of S(IV) in the presence of nitrogen oxides and thiosulfate, as a refinement of the Ajdari mechanism.¹⁹ The proposed reaction sets follow the work carried out by Littlejohn et al.,² in which sulfite radicals are suggested to play a key role in the system. Adjustments are made to the set proposed by Littlejohn et al.,² which will be discussed later, to account for experimental observations. In total, five mechanisms with varying complexity are evaluated. A reference set is proposed that applies the original mechanism (described in Table 2), to demonstrate the gap between the established kinetic data and the observed experimental results. Two reaction sets with different levels of complexity are proposed to incorporate the impact of NO₂ on S(IV) oxidation: (i) the sulfur reduction reaction (SRR), which includes a set of S(IV) radical reactions; and (ii) the global radical reaction (GRR), which includes one global radical reaction. Finally, two radical-scavenging reaction sets are proposed to complement the SRR in the presence of

thiosulfate: (i) the thiosulfate regeneration reaction (ThRX), and (ii) the thiosulfate radical reaction (ThRR).

The kinetics of the proposed reactions in the SRR, ThRX, and ThRR are based on reaction stoichiometry. Accounting for the presence of radical species in these mechanisms is simplified with a steady-state approximation, whereby the concentration of radical intermediates is assumed to remain constant. By allowing for equal rates of radical formation and consumption, the overall reaction rate can be derived in terms of known species concentrations. The rate coefficient is iteratively determined to minimize the error between the S(IV) concentrations obtained from the model and experiments. The Root Mean Square Deviation (RMSD) is used to define the error for n data points, considering each time step i using the following formula

$$\delta = \sqrt{\frac{\sum_{i=1}^n (C_{S(IV),mod,i} - C_{S(IV),exp,i})^2}{n}} \quad (9)$$

Meanwhile, in the GRR set, S(IV) concentration profile is constructed as the differential S(IV) consumption between Investigation 4 and the reference case, as described by

$$C_{GRR} = C_{S(IV)_{Inv4}} - C_{S(IV)_{RefCase}} \quad (10)$$

The resulting profile is considered as a product of a general reaction, which defines the amount of S(IV) consumed by the unknown radical mechanism. The reaction order with respect to SO₃²⁻ is determined using C_{GRR} and its rate of decay. A similar iterative procedure with eq 9 is then carried out to determine the rate coefficient.

4. RESULTS AND DISCUSSION

4.1. Mass Transfer Parameter Fitting. The gas–liquid interaction plays a critical role in the multiphase system. An important parameter to describe this interaction is the contact area, which is dependent upon the average bubble size. This parameter is estimated by simulating a system with constant flow of NO₂ into water and then fitting the concentration profile to the available experimental data. The kinetics of NO₂ dissolution (R20) and its corresponding Henry's law coefficient are well-documented in the literature,^{34–36} as is the dissociation of its aqueous product HNO₂ (R21). Established knowledge of this system provides a controlled environment that enables approximation of an unknown bubble diameter. In Table 5, the mean percentage error between modeled NO₂ outlet concentrations obtained for different bubble sizes and the measured concentration from Investigation 0 are summarized. It can be concluded that within a reasonable range for bubble size in a laboratory-scale reactor setup (1–6 mm),^{37,38} the calculated NO₂ absorption levels remain within the experimental measurement. Considering the lack of sparger in the setup and the observed large bubble formation, a value of 5 mm is chosen as it provides reasonable agreement with the experimental data while being consistent with qualitative observation.

4.2. Reaction Mechanism and Kinetics. Two reaction sets are proposed to address the radical-induced S(IV) oxidation. The SRR set is constructed to capture the effect of SO₃^{•-} radicals on S(IV) oxidation in the presence of NO_{2(aq)}. The pathways are based on R5–R14, wherein modifications are made to simplify the computational steps. Reactions RSSR1 and RSSR2 are identical to R5 and R9, which are considered to be the key reactions producing the

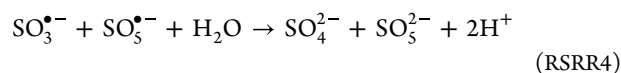
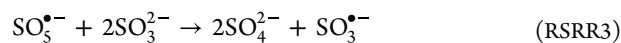
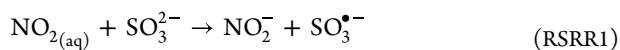
Table 4. Proposed Reaction Sets To Complement The Reaction Mechanism Listed in Table 2

reaction set	gas species		liquid species		new reactions
	O ₂	NO ₂	S(IV)	S ₂ O ₃ ²⁻	
reference	●		●		N/A
	●	●	●		NO _{2(aq)} + SO ₃ ²⁻ → NO ₂ ⁻ + SO ₃ ^{•-}
SRR	●	●	●		SO ₃ ^{•-} + O ₂ → SO ₅ ^{•-} SO ₅ ^{•-} + 2SO ₃ ²⁻ → 2SO ₄ ²⁻ + SO ₃ ^{•-} SO ₃ ^{•-} + SO ₅ ^{•-} + H ₂ O → SO ₄ ²⁻ + SO ₅ ²⁻ + 2H ⁺
GRR	●	●	●		2NO _{2(aq)} + 7SO ₃ ²⁻ + H ₂ O + 3O ₂ → 2NO ₂ ⁻ + 7SO ₄ ²⁻ + 2H ⁺ SRR + SO ₃ ^{•-} + S ₂ O ₃ ²⁻ → SO ₃ ²⁻ + S ₂ O ₃ ^{•-}
ThRX	●	●	●	●	S ₂ O ₃ ^{•-} + S ₂ O ₃ ^{•-} → S ₄ O ₆ ²⁻ S ₄ O ₆ ²⁻ + SO ₃ ²⁻ → SO ₄ ²⁻ + S ₂ O ₃ ²⁻ + SO ₂
ThRR	●	●	●	●	SRR + SO ₃ ^{•-} + S ₂ O ₃ ²⁻ → SO ₃ ²⁻ + S ₂ O ₃ ^{•-} 2S ₂ O ₃ ^{•-} + 2O ₂ → SO ₄ ²⁻ + 3SO ₂

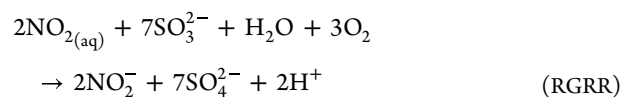
Table 5. Mean Percentage Error of Modeled NO₂ Outlet Concentrations for the Different Bubble Diameters, as Compared with Investigation 0

bubble diameter	mean percentage error (%)
1 mm	1
3 mm	4
5 mm	6
6 mm	8

initiating radicals SO₃^{•-} and SO₅^{•-}. Reaction RSS2, which is a combination of R11 and R12, contributes to the rapid consumption of SO₃²⁻. A termination reaction (RSSR4) is included to define the termination step of the radicals.



The concentration of radicals remains constant throughout the runs, which confirms the steady-state assumption. In the GRR set, a global radical reaction is derived from RS–R14 and represented as



The overall reaction mechanism yields three radical species on the left-hand side and S₂O₆²⁻ on the right-hand side. To avoid explicitly modeling radical species, the radicals are accounted for in the reaction as SO₃^{•-}.² The presence of dithionate (S₂O₆²⁻) formed through R6 is omitted as it was not detected in the experiment, so dithionate is aggregated into SO₄²⁻ to

Table 6. Proposed Reactions, Kinetic Rate Expressions, and Residual Errors of the Fitting Procedure for the Reaction Sets

reaction set	reaction	kinetic rate expression (mol/m ³ /s)	δ _{C_{(s(IV))}}
reference case	2SO ₃ ²⁻ + O _{2(aq)} → 2SO ₄ ²⁻	r ₂ = 6 × 10 ⁻⁶ C _{H⁺} ^{-0.16} C _{SO₃²⁻}	0.28
	NO _{2(aq)} + SO ₃ ²⁻ → NO ₂ ⁻ + SO ₃ ^{•-}	r _{RSR1} = 2 C _{NO₂} C _{SO₃²⁻}	
SRR	SO ₃ ^{•-} + O ₂ → SO ₅ ^{•-}	r _{RSR2} = 2 C _{SO₃^{•-}} C _{O₂}	0.06
	SO ₅ ^{•-} + 2SO ₃ ²⁻ → 2SO ₄ ²⁻ + SO ₃ ^{•-}	r _{RSR3} = 1.9 C _{SO₅^{•-}} C _{SO₃²⁻} ²	
	SO ₃ ^{•-} + SO ₅ ^{•-} + H ₂ O → SO ₄ ²⁻ + SO ₅ ²⁻ + 2H ⁺	r _{RSR4} = 0.2 C _{SO₃^{•-}} C _{SO₅^{•-}}	
GRR	2NO _{2(aq)} + 7SO ₃ ²⁻ + H ₂ O + 3O ₂ → 2NO ₂ ⁻ + 7SO ₄ ²⁻ + 2H ⁺	r _{GRR} = 1.24 × 10 ⁻⁴ C _{SO₃²⁻}	1.07
	SO ₃ ^{•-} + S ₂ O ₃ ²⁻ → SO ₃ ²⁻ + S ₂ O ₃ ^{•-}	r _{ThRX1} = 113.5 C _{SO₃^{•-}} C _{S₂O₃²⁻}	
ThRX	S ₂ O ₃ ^{•-} + S ₂ O ₃ ^{•-} → S ₄ O ₆ ²⁻	r _{ThRX2} = 91.62 C _{S₂O₃^{•-}} ²	2.41
	S ₄ O ₆ ²⁻ + SO ₃ ²⁻ → SO ₄ ²⁻ + S ₂ O ₃ ²⁻ + SO ₂	r _{ThRX3} = 97.68 C _{S₄O₆²⁻} C _{SO₃²⁻}	
	SO ₃ ^{•-} + S ₂ O ₃ ²⁻ → SO ₃ ²⁻ + S ₂ O ₃ ^{•-}	r _{ThRR1} = 0.32 C _{SO₃^{•-}} C _{S₂O₃²⁻}	
ThRR	2S ₂ O ₃ ^{•-} + 2O ₂ → SO ₄ ²⁻ + 3SO ₂	r _{ThRR2} = 0.99 C _{S₂O₃^{•-}} ² C _{O₂}	2.41

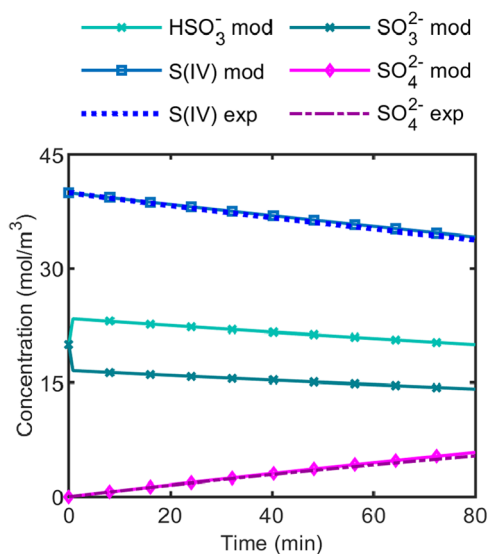
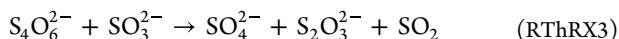
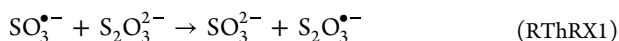


Figure 4. Liquid concentration profiles of sulfur oxides estimated by modeling the reference mechanism (mod), in comparison to those from Investigation 1 (exp).

maintain the sulfur atom balance. The concentration of $\text{NO}_{2(\text{aq})}$ is not included in the rate expression, as its concentration is constant during the run, indicating a mass transfer-controlled process.

The thiosulfate reactions reported by Mo et al.²⁸ based on the work of Chang and Brna²⁹ form the basis for the pathway of ThRX. The mechanism requires the SRR set to remain active, in order to capture the dynamics between radical propagation and radical scavenging. The mechanism involves polythionate as an intermediate, which further reacts to regenerate thiosulfate and form sulfate. Thus, the following reactions are formulated



The modeling results reveal that polythionate and thiosulfate regeneration has no significant effect on the system. Therefore, the following simplified reaction set (named ThRR) is proposed

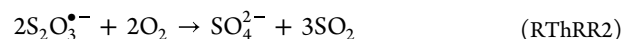
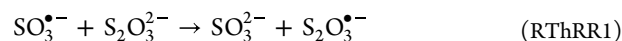


Table 6 summarizes the kinetic rate expressions obtained from the fitting of the proposed reactions, along with the residual error ($\delta_{C_{S(\text{IV})}}$) between the calculated and measured S(IV) concentrations. The following subsections discuss the performance of each reaction set, starting with the reference mechanism without a specific subset for S(IV) ion oxidation in the presence of nitrogen.

4.2.1. Reference Mechanism. The reference mechanism gives the S(IV) oxidation rate for a system that contains only O_2 in the gas phase and S(IV) ions in the liquid phase, i.e., there are no nitrogen species present. The initial concentration is an equimolar distribution of HSO_3^- and SO_3^{2-} along with 3% O_2 , with a maintained pH of 7. The rate coefficient for R2 (fitted according to the procedure described in Subsection 3.3) is 2 orders of magnitude lower than that reported by Beilke et al., which can be attributed to the sensitivity of R2 to variations in the experimental setup.^{10,11}

Figure 4 shows the calculated and measured liquid concentrations from Investigation 1, in which the model captures effectively the measured liquid concentration. As suggested by the rate expression, HSO_3^- is not directly oxidized in the reaction. Instead, SO_3^{2-} is the reacting species, as has been confirmed by several groups.^{23,24,39} The experimental results reported by Johansson et al.⁴ show good agreement, as the level of HSO_3^- remains relatively constant throughout the runs, and the rate of SO_3^{2-} depletion is the same as that of sulfate production. The model predicts a slight decrease in HSO_3^- to sustain the equimolar ratio of S(IV) ions at a constant pH of 7.

Figure 5a shows the experimental measurements Investigation 4, which include $\text{NO}_{2(\text{g})}$, and the modeling results using the reference mechanism. The reference kinetic model does not capture the significant increase in S(IV) oxidation rate in the presence of $\text{NO}_{2(\text{g})}$. The rate remains driven by R2,

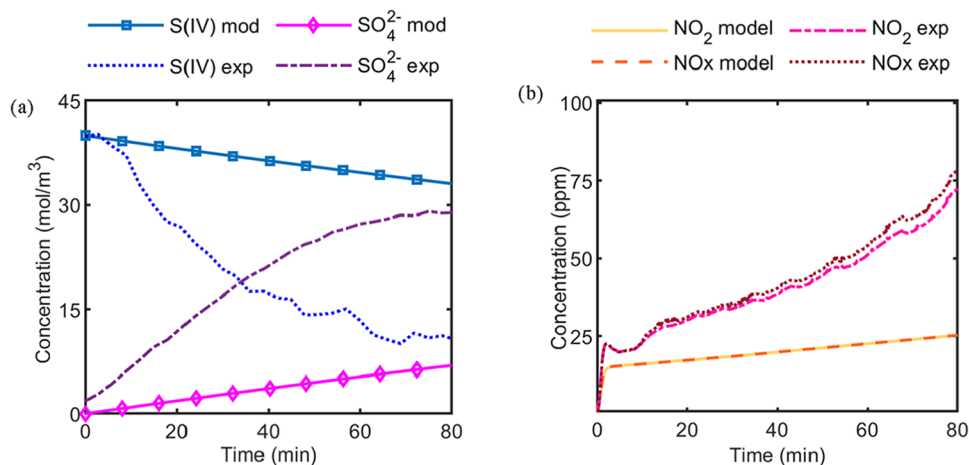


Figure 5. Liquid (a) and gaseous (b) concentration profiles of sulfur oxides and nitrogen oxides, respectively, estimated by modeling the reference mechanism (mod), in comparison to the results from Investigation 4 (exp).

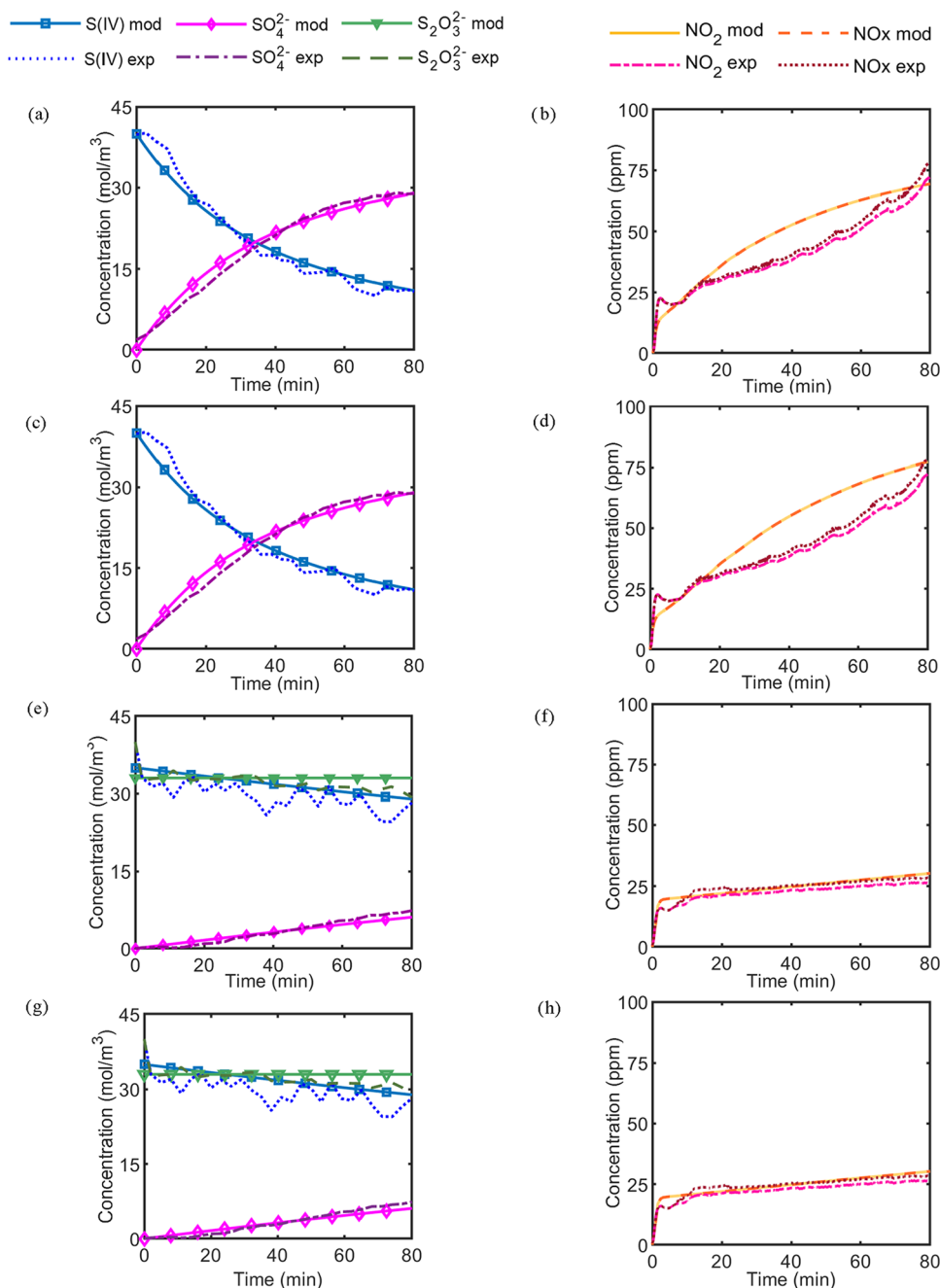


Figure 6. Concentration profiles of sulfur oxides and nitrogen oxides in the liquid and gaseous phases, respectively, for: (a) and (b) SRR; (c) and (d) GRR; (e) and (f) ThRX; (g) and (h) ThRR. mod, Modeled; exp, Experimental.

with minor contributions from R3 and R4, which further confirms the substantial gap between the reported kinetics and observed reaction rate for S(IV) oxidation by NO₂.

The Hatta number for reactions that involve NO_{2(aq)} is determined using eq 5, and a value of ~500 is obtained for R3 and R4, which confirms the assumption of an instantaneous regime and enhanced mass transfer by reaction. Since the NO₂ absorption rate is governed by the S(IV) concentration, the modeled outlet NO_{2(g)} concentration shown in Figure 5b is much lower compared to that obtained in the experiment. This signifies a higher absorption level, in accordance with the continuous presence of S(IV) in the liquid phase.

4.2.2. NO₂ Radical Chain Mechanism. The calculated and measured liquid concentrations from SRR set and Investigation

4 are shown in Figure 6a. The level of agreement between the modeled and experimental results is good ($\delta_{C_{S(IV)}} = 1.07$). Figure 6b shows the calculated and measured gas outlet concentrations from Investigation 4. The modeled gaseous concentration shows a different trend compared to the experimental result, which is suspected to be an effect of the pH maintenance method in the experiment, where strong base is periodically added. However, the general agreement in terms of absorption levels shows that the model can capture the dependency of the NO₂ absorption rate on the S(IV) concentration.

For the GRR set, the resulting concentration profile determines the reaction order, calculated by plotting the rate coefficient against concentration. An iterative algorithm was

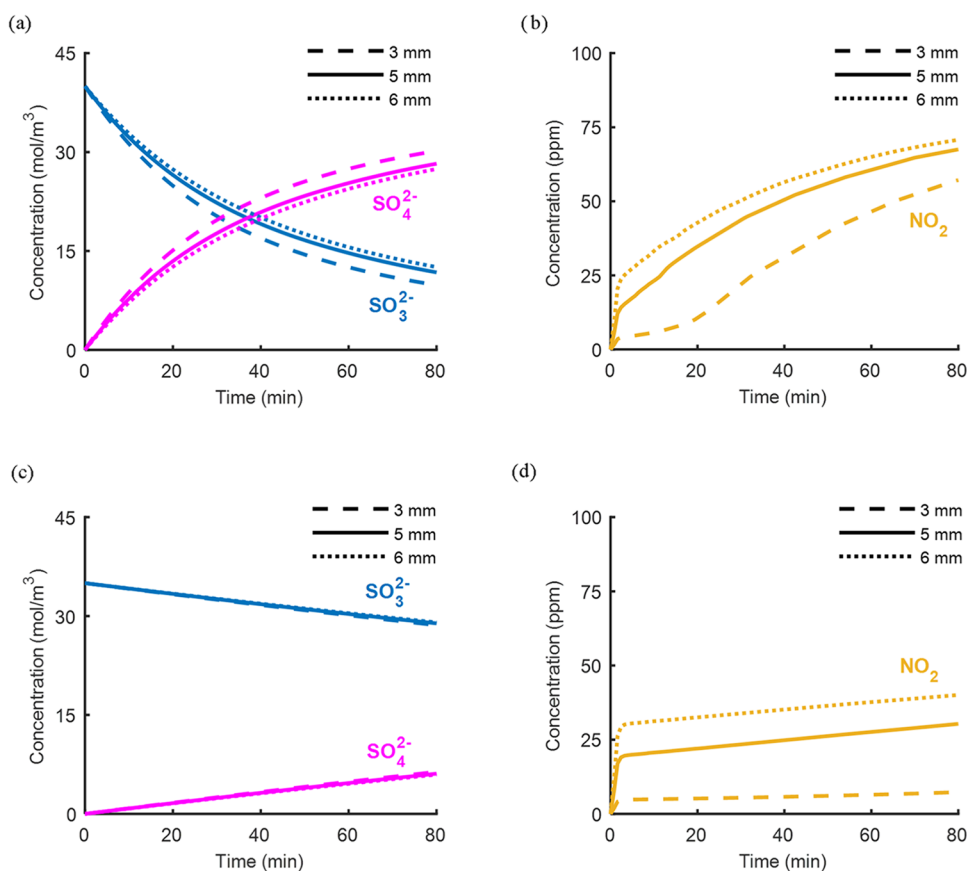


Figure 7. Effects of bubble diameter on the concentration profiles for the: (a) SRR liquid phase; (b) SRR gas phase; (c) ThRX liquid phase; (d) ThRX gas phase.

used to obtain the rate coefficient that gives the concentration profiles shown in Figure 6c and Figure 6d. A minor difference can be observed between the liquid concentration profile obtained from the GRR and the SRR, in which the SRR initially shows a faster reaction that decelerates with time, while the rate observed in the GRR is relatively constant throughout the run. This is a result of the dynamics of the reaction intermediates, which are not captured with the GRR mechanism, as the kinetics are defined with a single global rate expression. However, since both mechanisms show good agreement with the experimental data, the GRR would be favorable for process modeling owing to the absence of radical species.

4.2.3. Thiosulfate-Scavenging Mechanism. The calculated liquid concentrations in Figure 6e show a good approximation to the measured S(IV) and sulfate concentrations. However, the measured thiosulfate consumption is not captured by the model, and its concentration remains constant over the timespan. The calculated concentration profile reveals that only $0.54 \mu\text{mol}$ of thiosulfate was consumed by R115, which is well below the threshold of practical significance. Regenerated thiosulfate was quantified as being as low as $0.27 \mu\text{mol}$, contributing little to sustaining the presence of thiosulfate. Furthermore, the level of polythionates was predicted to approach zero. Figure 6f illustrates the modeled outlet gas concentration, with an initial $\text{NO}_{2(g)}$ outlet concentration of 20 ppm, which increases to 30 ppm by the end of the run, showing a good fit to the experimental data.

The negligible concentration of polythionate in the modeled results are in agreement with the experimental results, where

no polythionates were observed in the final liquid solution. In addition, the minor contribution of thiosulfate regeneration undermines its relevance for the system, so the possibility of adapting to a simplified reaction set is considered in the ThRR. Figure 6g,6h show identical results to those for the ThRX mechanism, confirming that a simplified pathway provides a satisfactory confirmation of the thiosulfate radical-scavenging mechanism.

4.3. Sensitivity Analysis. The fitting of mass transfer parameters in Section 4.1 is crucial, as the bubble diameters determine the interfacial area, which in turn governs the molar flux between the gas and liquid phases. This step relies heavily on the NO_2 outlet concentration data, where the gas analyzer is reported to give a $\pm 5\%$ measurement error.⁴⁰ Therefore, a sensitivity analysis is performed to evaluate the effect of measurement errors on the obtained concentration profile for each mechanism. Although the boundary values for bubble size are suggested to be 1 mm and 6 mm (see Section 4.1), the applied mass transfer coefficient correlation is valid for a bubble diameter >2.5 mm. Thus, the resulting profile is evaluated for diameters of 3 mm and 6 mm.

Figure 7 shows the concentration profiles for different bubble diameters. In general, varying the bubble size affects the liquid concentration only to a minor extent. More-prominent effects are observed for the gaseous concentration, as a diameter of 3 mm yields a significantly higher absorption level. A smaller bubble size leads to a high level of absorbed NO_2 , which is much higher compared to its corresponding S(IV) ion concentration, signifying that a different regime needs to be

considered when evaluating the model under such operating condition.

5. CONCLUSION

The present work addresses the gap in the knowledge regarding a reaction mechanism to describe liquid-phase S(IV) oxidation by dissolved NO₂, focusing on the roles of radical species and their scavenging mechanism. Reaction sets for sulfite oxidation and thiosulfate scavenging in sulfur/nitrogen solutions are proposed. Kinetic parameters are derived from fitting to the most recent measurements. The resulting mechanisms describe the changes in concentrations of the important nitrogen and sulfur species, both in the liquid and gaseous phases. The model predicts both the S(IV) ion concentration and the NO₂ absorption rates, which are important for ensuring reliable process simulations and for showing an accurate correlation between the two parameters. This enables a reasonable prediction of the aqueous concentration and NO₂ absorption performance, which will be beneficial in optimizing the absorption process by providing an estimation of the additive requirement.

A simplified sulfite oxidation mechanism (GRR) is formulated by excluding radical species. This allows incorporation into the process modeling software, while avoiding uncertainties related to the properties of radicals. It has also been shown that the reported mechanism for thiosulfate scavenging, during which polythionate intermediates are formed and thiosulfate is regenerated, can be simplified to produce only SO₄²⁻ as the final product.

The hydrodynamics of the experimental setup can be a source of uncertainties for the resulting concentration profile. The sensitivity analysis results show that the prediction of NO₂ absorption is highly influenced by mass transfer parameters, i.e., bubble size, while only minor dependency is observed for liquid concentrations.

■ ASSOCIATED CONTENT

SI Supporting Information

The Supporting Information is available free of charge at <https://pubs.acs.org/doi/10.1021/acs.iecr.5c03944>.

Detailed liquid and gas-phase concentration, as well as the sensitivity analysis results for all reaction sets are presented as Supporting Information (PDF)

■ AUTHOR INFORMATION

Corresponding Author

Rosa C. Aprilia – Department of Space, Earth, and Environment, Chalmers University of Technology, SE-412 96 Gothenburg, Sweden; orcid.org/0009-0005-1754-9395; Email: aprilia@chalmers.se

Authors

Jakob Johansson – Department of Space, Earth, and Environment, Chalmers University of Technology, SE-412 96 Gothenburg, Sweden; orcid.org/0000-0001-8011-7783

Fredrik Normann – Department of Space, Earth, and Environment, Chalmers University of Technology, SE-412 96 Gothenburg, Sweden

Complete contact information is available at: <https://pubs.acs.org/10.1021/acs.iecr.5c03944>

Notes

The authors declare no competing financial interest.

■ ACKNOWLEDGMENTS

This work was supported by Swedish Energy Agency (grant number 50368-1) and Nouryon Pulp and Performance Chemicals AB (grant number 46438-1).

■ REFERENCES

- (1) Takeuchi, H.; Takahashi, K.; Kizawa, N. Absorption of Nitrogen Dioxide in Sodium Sulfite Solution from Air as a Diluent. *Ind. Eng. Chem. Process Des. Dev.* **1977**, *16* (4), 486–490.
- (2) Littlejohn, D.; Wang, Y.; Chang, S. G. Oxidation of aqueous sulfite ion by nitrogen dioxide. *Environ. Sci. Technol.* **1993**, *27* (10), 2162–2167.
- (3) Clifton, C. L.; Altstein, N.; Huie, R. E. Rate constant for the reaction of nitrogen dioxide with sulfur(IV) over the pH range 5.3–13. *Environ. Sci. Technol.* **1988**, *22* (5), 586–589.
- (4) Johansson, J.; Wagaarachchige, J. D.; Normann, F.; Idris, Z.; Haugen, E. R.; Halstensen, M.; Jinadasa, W.; Jens, K. J.; Andersson, K. Influence of Nitrogen Dioxide Adsorption on the Sulfite Oxidation Rate in the Presence of Oxygen: Online Raman Measurements. *Ind. Eng. Chem. Res.* **2023**, *62* (49), 21048–21056.
- (5) Johansson, J.; Department of Space, Earth, and Environment. Absorption Based Systems for Co-removal of Nitrogen Oxides and Sulfur Oxides from Flue Gases; PhD Thesis; Chalmers University of Technology 2022.
- (6) Schmid, D.; Hupa, M.; Paavola, M.; Vuorinen, I.; Lehtikoinen, A.; Karlström, O. Role of Thiosulfate in NO₂ Absorption in Aqueous Sulfite Solutions. *Ind. Eng. Chem. Res.* **2023**, *62* (1), 105–110.
- (7) Neta, P.; Huie, R. E. Free-radical chemistry of sulfite. *Environ. Health Perspect.* **1985**, *64*, 209–217.
- (8) Johansson, J.; Heijnesson Hultén, A.; Normann, F.; Andersson, K. Simultaneous Removal of NO_x and SO_x from Flue Gases Using ClO₂: Process Scaling and Modeling Simulations. *Ind. Eng. Chem. Res.* **2021**, *60* (4), 1774–1783.
- (9) Akita, K.; Yoshida, F. Gas Holdup and Volumetric Mass Transfer Coefficient in Bubble Columns. Effects of Liquid Properties. *Ind. Eng. Chem. Process Des. Dev.* **1973**, *12* (1), 76–80.
- (10) Sivaji, K.; Murty, G. S. R. N. Kinetics of sulfite oxidation reaction. *Ind. Eng. Chem. Fundam.* **1982**, *21* (4), 344–352.
- (11) Linek, V.; Mayrhoferová, J. The kinetics of oxidation of aqueous sodium sulphite solution. *Chem. Eng. Sci.* **1970**, *25* (5), 787–800.
- (12) Ermakov, A. N.; Poskrebyshev, G.; Pural, A. P. Sulfite Oxidation: The State-of-the-Art of the Problem. *Kinet. Catal.* **1997**, *38*, 295–308.
- (13) Ellison, T. K.; Eckert, C. A. The oxidation of aqueous sulfur dioxide. 4. The influence of nitrogen dioxide at low pH. *J. Phys. Chem. A* **1984**, *88* (11), 2335–2339.
- (14) Sapkota, V. N. A.; Fine, N. A.; Rochelle, G. T. NO₂-Catalyzed Sulfite Oxidation. *Ind. Eng. Chem. Res.* **2015**, *54* (17), 4815–4822.
- (15) Ajdari, S.; Normann, F.; Andersson, K.; Johansson, F. Modeling the Nitrogen and Sulfur Chemistry in Pressurized Flue Gas Systems. *Ind. Eng. Chem. Res.* **2015**, *54* (4), 1216–1227.
- (16) Yagi, S.; Inoue, H. The absorption of oxygen into sodium sulphite solution. *Chem. Eng. Sci.* **1962**, *17* (6), 411–421.
- (17) Beilke, S.; Lamb, D.; Müller, J. On the uncatalyzed oxidation of atmospheric SO₂ by oxygen in aqueous systems. *Atmos. Environ.* **1975**, *9* (12), 1083–1090.
- (18) Rochelle, G. T.; Owens, D. R.; Chang, J. C. S.; Bma, T. G. Thiosulfate as an Oxidation Inhibitor in Flue Gas Desulfurization Processes: A Review of R&D Results. *J. Air Pollut. Control Assoc.* **1986**, *36* (10), 1138–1146.
- (19) Ajdari, S.; Normann, F.; Andersson, K.; Johansson, F. Reduced Mechanism for Nitrogen and Sulfur Chemistry in Pressurized Flue Gas Systems. *Ind. Eng. Chem. Res.* **2016**, *55* (19), 5514–5525.

- (20) Beilke, S.; Gravenhorst, G. Heterogeneous SO₂-oxidation in the droplet phase. *Atmos. Environ.* **1978**, *12* (1), 231–239.
- (21) Winkelmann, D. Die elektrochemische Messung der Oxidationsgeschwindigkeit von Na₂SO₃ durch gelösten Sauerstoff. *Z. Elektrochem.* **1955**, *59*, 891–895.
- (22) Linek, V.; Vacek, V. Chemical engineering use of catalyzed sulfite oxidation kinetics for the determination of mass transfer characteristics of gas–liquid contactors. *Chem. Eng. Sci.* **1981**, *36* (11), 1747–1768.
- (23) Fuller, E. C.; Crist, R. H. The Rate of Oxidation of Sulfite Ions by Oxygen. *J. Am. Chem. Soc.* **1941**, *63* (6), 1644–1650.
- (24) Miller, J. M.; de Pena, R. G. Contribution of scavenged sulfur dioxide to the sulfate content of rain water. *J. Geophys. Res.* **1972**, *77* (30), 5905–5916.
- (25) Scott, W. D.; Hobbs, P. V. The Formation of Sulfate in Water Droplets. *J. Atmos. Sci.* **1967**, *24* (1), 54–57.
- (26) Senjo, T.; Kobayashi, M.; Kubota Kasui Corp. Process for removing nitrogen oxides from exhaust gases. US Patent US4029739A, 1976.
- (27) Shen, C. H.; Rochelle, G. T. Nitrogen Dioxide Absorption and Sulfite Oxidation in Aqueous Sulfite. *Environ. Sci. Technol.* **1998**, *32* (13), 1994–2003.
- (28) Mo, J.-s.; Wu, Z.-b.; Cheng, C.-j.; Guan, B.-h.; Zhao, W.-r. Oxidation inhibition of sulfite in dual alkali flue gas desulfurization system. *J. Environ. Sci.* **2007**, *19* (2), 226–231.
- (29) Chang, J. C. S.; Brna, T. G. Pilot testing of sodium thiosulfate. *Environ. Prog.* **1986**, *5* (4), 225–233.
- (30) Normann, F.; Jansson, E.; Petersson, T.; Andersson, K. Nitrogen and sulphur chemistry in pressurised flue gas systems: A comparison of modelling and experiments. *Int. J. Greenhouse Gas Control* **2013**, *12*, 26–34.
- (31) Kawase, Y.; Moo-Young, M. Correlations for liquid-phase mass transfer coefficients in bubble column reactors with newtonian and non-newtonian fluids. *Can. J. Chem. Eng.* **1992**, *70* (1), 48–54.
- (32) Cho, J. S.; Wakao, N. Determination of liquid-side and gas-side volumetric mass transfer coefficients in a bubble column. *J. Chem. Eng. Jpn.* **1988**, *21* (6), 576–581.
- (33) Versteeg, G. F.; Kuipers, J. A. M.; Van Beckum, F. P. H.; Van Swaaij, W. P. M. Mass transfer with complex reversible chemical reactions—II. parallel reversible chemical reactions. *Chem. Eng. Sci.* **1990**, *45* (1), 183–197.
- (34) Lee, Y. N.; Schwartz, S. E. Reaction kinetics of nitrogen dioxide with liquid water at low partial pressure. *J. Phys. Chem. A* **1981**, *85* (7), 840–848.
- (35) Schwartz, S. E.; White, W. H. Solubility equilibria of the nitrogen oxides and oxyacids in dilute aqueous solution *Adv. Environ. Sci. Eng.* 1981; Vol. 4.
- (36) Park, J. Y.; Lee, Y. N. Solubility and decomposition kinetics of nitrous acid in aqueous solution. *J. Phys. Chem. A* **1988**, *92* (22), 6294–6302.
- (37) Fadavi, A.; Chisti, Y.; Chriaštel, L. Bubble size in a forced circulation loop reactor. *J. Chem. Technol. Biotechnol.* **2008**, *83* (1), 105–108.
- (38) Grau, R. A.; Heiskanen, K. Bubble size distribution in laboratory scale flotation cells. *Miner. Eng.* **2005**, *18* (12), 1164–1172.
- (39) McKay, H. A. C. The atmospheric oxidation of sulphur dioxide in water droplets in presence of ammonia. *Atmos. Environ.* **1971**, *5* (1), 7–14.
- (40) Testo. Testo 350 - Multifunction Measuring Instrument, 2025. <https://www.testo.com/en-UK/testo-350/p/0632-3510#tab-technicalData>.